Assessment of Mould Growth on Building Materials using Spatial and Frequency Domain Analysis Techniques

A. M. Aibinu[1], M. J. E. Salami[1], A. Shafie[1], M. Ali [2] and I. A. Bamgbopa[2]
[1]Department of Mechatronics, Kulliyyah of Engineering (KENG),
[2]Department of Building Technology and Engineering,
Kulliyyah of Architecture and Environmental Design (KAED),
International Islamic University Malaysia (IIUM)
P O Box 53100 Gombak, Malaysia.

Abstract

The phenomenon of Sick Building Syndrome (SBS), Building Related Illness (BRI) and some other indoor related diseases have been attributed to mould and fungi exposure in the indoor environment. Despite the growing concern over mould and fungi infestations on building materials, little has been reported in the literature on the development of an objective tool and criteria for measuring and characterizing the shape and the level of severity of such parasitic phenomenon.

In this paper, an objective based approach of mould and fungi growth assessment using spatial and frequency domain information is proposed. The spatial domain analysis of the acquired Mould Infested Images (MII) is achieved using Ratio Test (RT), Compactness Test (CT) and Visual Test (VT) while the frequency domain analysis uses the popular Discrete Fourier Transform (DFT) implemented in the form of Fast Fourier Transform (FFT) in analyzing the boundary pixel sequence. The resulting frequency components (Fourier Descriptors (FD)) can now be analyzed or stored for reconstruction purposes.

Application of structural similarity measures on the reconstructed MII in spatial domain shows that the use of relative low number of FD is sufficient for analyzing, characterizing and reconstruction of the original spatial domain boundary pixels.

Keywords: Building Related Illness (BRI); Digital Image Processing; Mould; Sick Building Syndrome (SBS); Discrete Fourier Transform (DFT).

1. Introduction

The word"Mould" is commonly used to describe visible fungal growth and forms of microbial contamination [1], [2], [4]. Moulds and fungi have been commonly referred to interchangeably in various literatures and is a known fact that "all moulds are fungi, but not all fungi are moulds" [5]. Moulds are ubiquitous and are essential decomposers of organic substances necessary for sustaining plant and animal life [6].

Moulds (Fungi) are microscopic in size and their spores travel through the air. Their growth and survival on surfaces is determined by the micro environmental conditions of both the materials and the indoor space; such as the high humidity, temperature, Radiation and Light, Nutrient, Oxygen, PH level and particularly the water content of the material/substrate (water activity) [1], [7], [8]. They strive on virtually all building materials and surfaces (both organic and inorganic) [9], [10], causing degradation of materials and components of buildings materials (see Fig. 1).

Once mould infects a surface, it is completely impossible to eradicate or remove them due to the protective layer formed by the moulds itself [1], [8]. When moulds are exposed to ultraviolet light or toxic chemicals such as bleach, only the top layer of the moulds is usually killed. As long as the original spore is unaffected, it will continue to exist on the surface in a quiescent state; once additional moisture is present, the moulds will again reproduce and develop [8], [11]. Moulds growth appears in different colors and patterns. Three patterns of growth have been identified in the recent past, and these may be in form of moisture stains, radiate from spots or bloom around the damaged material [1], [12].

Fungi have the ability to evoke biological corrosion of building materials and thereby load the indoor air environment with harmful substances thus, contributing to a decline in the indoor air quality and creating BRI such as: SBS, allergic alveolitis, wheezing and Rhino-sinusitis, alteration in the brain blood flow, autonomic nerve function, brain waves, Asthma, worsen: concentration; attention; balance and memory [1], [14]–[21]. Moulds impact on human health depends on the nature of the species involved, the metabolic products produced by the species, the duration of exposure and the susceptibility of the individuals exposed [2].

Manuscript received July 5, 2009
Manuscript revised July 20, 2009

Similarly, moulds has the potential to cause degradation on virtually all building materials they colonize [25]; albeit, in the presence of appropriate microclimate to support their growth. Long term moulds growth has also been documented to cause deterioration of structural element [26]. Mould growth on building materials and components may range from small areas covering a few cm to a very large extent.

The growing awareness of the consequential health effect has in turn resulted into several litigation against designers, contractor's maintenance firms and local authorities particularly in USA and UK. Several cases involving moulds litigations are reported in [3].

Mould growth on building materials and components precursors a high concentration within the indoor, however incase of latent growth, IAQ assessment methods are often deployed [36] . Despite the growing concern over mould infestation on building materials and its presence in indoor environment, little has been reported on the development of an objective method and criteria for appraising level of damage of such unwanted phenomenon [37].

This publication describes an assessment of mould based on spatial and frequency domain technique. Also discussed in this paper are mould classification scheme and mould reconstruction technique. This paper is organized as follows; section 2 discusses shape modeling technique using DFT technique and its applicability to the present work. In section 3 the proposed framework is discussed while results obtained from both simulated and experimental images is contained in 4. Conclusion and recommendation is as contained in section 5.

2. Review of Shape Analysis and Fourier Descriptor

Shape analysis and recognition has been an area of keen research interest within the last few decades. The use of shape information for analysis, diagnosis, information retrieval has been applied to various fields, among which are medical image diagnosis, machine vision, content based retrieval system, information retrieval, surveillance, target recognition, industrial inspection, scene analysis, medical diagnosis etc.

Shape representation simply means characterizing a shape in terms of a set of features that makes it possible to reconstruct the shape exactly. It can also be described as the ability to characterize a shape to some degree of precision from a set of features [48].

These features are either based on shape boundary information only and are called contour based content or shape boundary information with the internal shape content and are normally referred to as region based content analysis [45], [48]. The contour based content shape analysis can be further subdivided into Closed Boundary Image (CBI) and Open Boundary Image (OBI), consider a shape with N boundary pixel, a CBI is defined as

$$Z_k = Z_{(N+k)}$$

Where $Z_k = (x_k; y_k)$. This is sometimes refered to as circularity property. Similarly an OBI is define as

$$\begin{aligned} Z_k &\neq Z_{(N+k)} \\ if\ Z_k &= 1 \\ then\ Z_{(k+N)} &= 0 \end{aligned} \tag{1}$$

The main distinguishing factor between CBI and OBI is the circularity property of the boundary pixel. Fig. 2a shows a typical CBI.

2.1 Shape Boundary Representation

In CBI analysis and representation, the given closed boundary shape can be represented by a finite sequence of complex or real numbers, these sequence of number are normally referred to as shape signatures [39], [41], [43], [44], [46]. Several shape boundary representation scheme has been suggested in literatures, these can broadly be divided into two major categories namely Complex-Valued Signature (CVS) and Real-Valued Signature (RVS).

1) Complex-Valued Signature (CVS):

Consider a CBI represented by coordinates system (Cartesian coordinate system), x and y shown in Fig. 2a, the complex coordinates of the CBI refers to the location (coordinates) of the boundary pixels (Fig. 2b). CVS representation and be divided into two types of representation, namely centered based complex coordinates [38], [40], [44]–[46] and Non centered based

$$z_k = x_k + iy_k \tag{2}$$

$$z_k = (x_k - x_c) + i(y_k - y_c) \tag{3}$$

complex coordinates [39], [43], [46] and are given by (2) and (3) respectively.

Where x_c and y_c refers to the coordinates of the center pixel.

(a) (b) (c)

Fig. 1. (a-c) Visible mould growth on building materials.

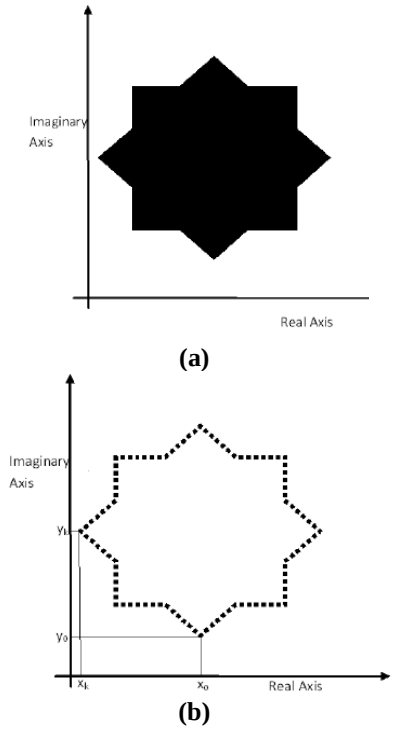

Fig. 2. (a) A typical CBI (b) Boundary pixels of CBI

2) Real-Valued Signature (RVS):

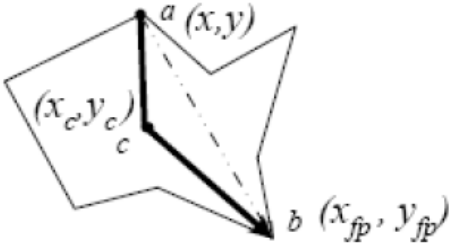

Fig. 3. FPD Signature Image [51]

- **Multidimensional System**

This refers to the coordinates of the boundary pixels being represented by two dimensional variables instead of the use of the use of the complex coordinates system. This involves representing the boundary in Cartesian form [43], [45]–[47]. The required representation is given as z_1 ; z_2 ; z_3 : : : z_N

Where $z_k = [x_k; y_k]$.

- **Centroid Distance**

The centroidal distance as a signature is a measure of the distance between the boundary pixels and the center pixel in an enclosed image [43], [45], [46]. This is a one dimensional signature and is mathematically represented as

$$r_k = \sqrt{(x_k - x_c)^2 + (y_k - y_c)^2} \qquad (4)$$

- **Curvature**

A curvature function is a function of angular changes of a boundary tangent. The curvature at any boundary point can always be expressed as a differentiation of successful tangent value in a window [38], [44]. Mathematically, this can be express as

$$\theta_k = \arctan \frac{y_k - y_{k-w}}{x_k - x_{k-w}} \qquad (5)$$

- **The Chord Length**

The chord length is defined as the distance between a boundary point and another boundary point within the shape. This distance must be perpendicular to the tangent at the starting point [44]. This measure of signature

overcomes the biased associated with the centered pixel, though it is highly sensitive to noise [44].

- **Farthest Point Distance (FPD)**

The FPD define as the value of the signature at a point *a* is the distance between the point (i.e point a) and the farthest distance from it. This is calculated by summing the Euclidean distance between points *a* and the centroid *c* to the distance between the centroid c and the farthest point [51].

$$FPD_k = \sqrt{(x_k - x_c)^2 + (y_k - y_c)^2} + \sqrt{(x_{fp} - x_c)^2 + (y_{fp} - y_c)^2} \quad (6)$$

Where (x_{fp} ; y_{fp}) is the coordinates of the farthest point from point k.

2.2 Fourier Descriptor (FD) its properties

The Fourier representation decomposes a shape boundary (normally CBI) into its frequency components (Fourier Descriptors) using the popular Fourier theory. These frequency components can be obtained by the application of Discrete Fourier Transform (DFT) on the signature. The DFT is normally expressed as :

$$A(k) = A(2\pi\frac{k}{N}) = \sum_{n=0}^{N-1} z[n]e^{-j2\pi\frac{k}{N}} \quad (7)$$

The complex valued coefficients AK; k = 0; 1; …….N ¡ 1, are called the Fourier Descriptors (FD) of the boundary [38], [47], [48]. The lower FD coefficients contain information about the general shape of the CBI while the high frequency FD coefficients contain information about small detail.

The inverse Fourier transform of these complex coefficients restores back the original boundary signature, z_k. That is, the corresponding Inverse Discrete Fourier Transform (IDFT) of the sequence A(k) gives a sequence z[n] defined on the interval 0 to N- 1 as

$$z[n] = \frac{1}{N}\sum_{k=0}^{N-1} A[k]e^{j2\pi\frac{k}{N}} \quad (8)$$

For k = 0; 1; 2: N- 1

Consider a CBI define by

$Z_k = [x_k, y_k]$; *where* $k = 1; 2;$ ……*N*

With FD A (k) for k = 0; 1; 2…….N - 1. The phase information of the FD is ignored and only the magnitude |A (k)| is used in computing some of the required properties of the CBI. These include

1) Rotational Invariance

If the CBI is rotated by Θ, a rotational invariance CBI is given by

$$e^{i\Theta}Z_k = Z_k, \ where \ k = 1, 2, 3 \ldots N$$

Rotational Invariance of the FD is obtained by dividing the magnitudes components by the DC component |A (0)| where A (0) is the first non-zero frequency components [50], [56], [57].

2) Translational Invariance

For a CBI to be translational invariance it simply means

$Z_{k+d} = Z_k$; where k = 1; 2; 3 …….N and d = x + iy

3) Size Invariance

A size or scale invariance CBI is mathematically given as

$$\alpha Z_k = Z_k, \ where \ k = 1, 2, 3 \ldots N \ and \ \alpha > 0$$

2.3 Various Applications of FD

Ear is a small sensory organ responsible for hearing. It has almost uniform color distribution even with reduced spatial resolution. Ear size can be used as a biometric identifier because the size does not change once the subject reaches an adult age. In [50], a robust rotational invariant method of FD called Generic Fourier Descriptor (GFD) was applied on a 2-D image of the ear. The acquired Cartesian image was firstly converted to polar coordinates and then normalized. The Polar Fourier Transform is then applied on the normalized image [50]. In making the GFD to be robust to rotation, phase information in the coefficients was ignored and the first magnitude of the coefficients was normalized by the area of the circle in which the polar image resides while all other magnitude values were normalized by the magnitude of the first coefficient. The GFD was highly robust to rotation and scale invariance but a small perturbation in translation significantly affects its performances.

A new Fourier descriptor shape signature was proposed in [51]. The proposed FPD captures information about an object's corner. The new object signature is based on the summation of two different distances, namely the distance between the point considered and the object center and secondly the distance between the object distance and the farthest point. To enhance the ability of the proposed

signature in capturing global detail, it was combined with other global descriptors. The result obtained when compared with other global descriptor methods like the curvature scale space and Zernike method shows superior performance. Despite the FPD Fourier based descriptor method performance, the method only works well for object with distinct edges and shapes.

Using the centroidal distance signature, a new method of FD called modified FD was applied to a set of rose flower images [52]. A new measurement of angular signature which uses a set of M highest FD signatures was proposed for image shape analysis. The proposed algorithm works well in analyzing star-shape flower extent but failed to analyze other shape features like roundness, ellipcity etc.

A three stage process for automatic classification of teeth in bitewing images using Bayesian classification and FD of the contour of the molar and the premolar teeth in a bitewing image was reported in [53]. The segmentation stage as the first stage in the process was used to obtain the contour of each of the individual tooth. The Bayesian classification in conjunction with the FD provides the initial classification of the teeth while the last stage used the spatial relationship between the images in order to solve and classify the image into appropriate classes. The maximum and minimum performance ratio achieved for pre classification of molar or premolar (in mandible and maxilla) is 95.5% and 72% respectively.

In [54], a new method of normalization of image signature prior to application of FD was proposed. The spatial domain centroidal signature was normalized by the centroidal distance of the first point. The resulting signature was found to be invariant to translation, rotation and scaling.

In [55], using discrete approximation of Fourier transform, a new algorithm for automatic side face portrait recognition based on FD was reported. The proposed algorithm was found to be rotational invariant and translational invariant so as to eliminate the influence cause by shooting angle deviation in the process of portrait photograph.

The use of ten low and high frequency components to describe pedestrian and vehicle shapes was reported in [56]. The complex and centroid coordinate's signatures were Fourier transformed and normalized before the application of support vector machine for classification. Result obtained by the application of the proposed algorithm on 500 pedestrians and 300 vehicles feature vectors shows that these 20 coefficients is sufficient to represent all the necessary features from the acquired images.

A novel method for Fourier based angular radius signature for shape descriptor in defect shape retrieval was reported in [57]. In the paper, it was shown that it is possible to combine the directional information of the boundary line with the Fourier shape description in order to obtain a descriptor with information on the frequency content of the boundary function as well as the boundary direction. The proposed descriptor outperforms ordinary FD in the retrieval of paper defect without increasing computational cost [57].

An efficient two-stage shape based leaf image retrieval system based on three simple sets of shape features was reported in [58]. Experimental results obtained by the application of the technique on 1400 leaf images from 140 plants shows that the proposed method of combining the centroid-contour distance curve with eccentricity and angle code histogram perform better than both the curvature scale space and the modified FD [58].

3. Proposed Mould Growth Analysis

A new global boundary information damage index and infestation tool based on FD is hereby proposed. The block diagram is as shown in Fig. 4 and detail discussion of the stages involved namely image preliminary processing stage, spatial domain analysis and frequency domain analysis.

3.1 Image Preliminary Processing Stage (IPPS)

Image Preliminary Processing Stage (IPPS) involve the following sub tasks:

1) Image (Data) Acquisition

This involves the use of digital camera to capture the Mould Infested Image (MII)).

2) Color Space Conversion:

The MII can be either a Red-Green-Blue (RGB) image or grey scale image. If it is an RGB image then it must be converted to grey scale image. If RGB images, then the grey scale intensity conversion is given as:

$$\begin{aligned} H &= \begin{cases} \theta, & for\ B \le G \\ 360-\theta, & for\ B > G \end{cases} \\ S &= 1 - \left\{ \frac{3}{R+G+B} \right\} min(R,G,B) \\ I &= \frac{1}{3}(R+G+B). \end{aligned} \tag{9}$$

where

$$\theta = cos^{-1}\left\{ \frac{[(R-G)+(R+B)]}{[(R-G)^2+(R-B)(G-B)]^{1/2}} \right\}$$

and

$$min(R,G,B)$$

Denotes the minimum of red, green and blue components of the input image [23]. After color space conversion, the intensity matrix will be extracted for further processing while the hue and saturation matrix are discarded

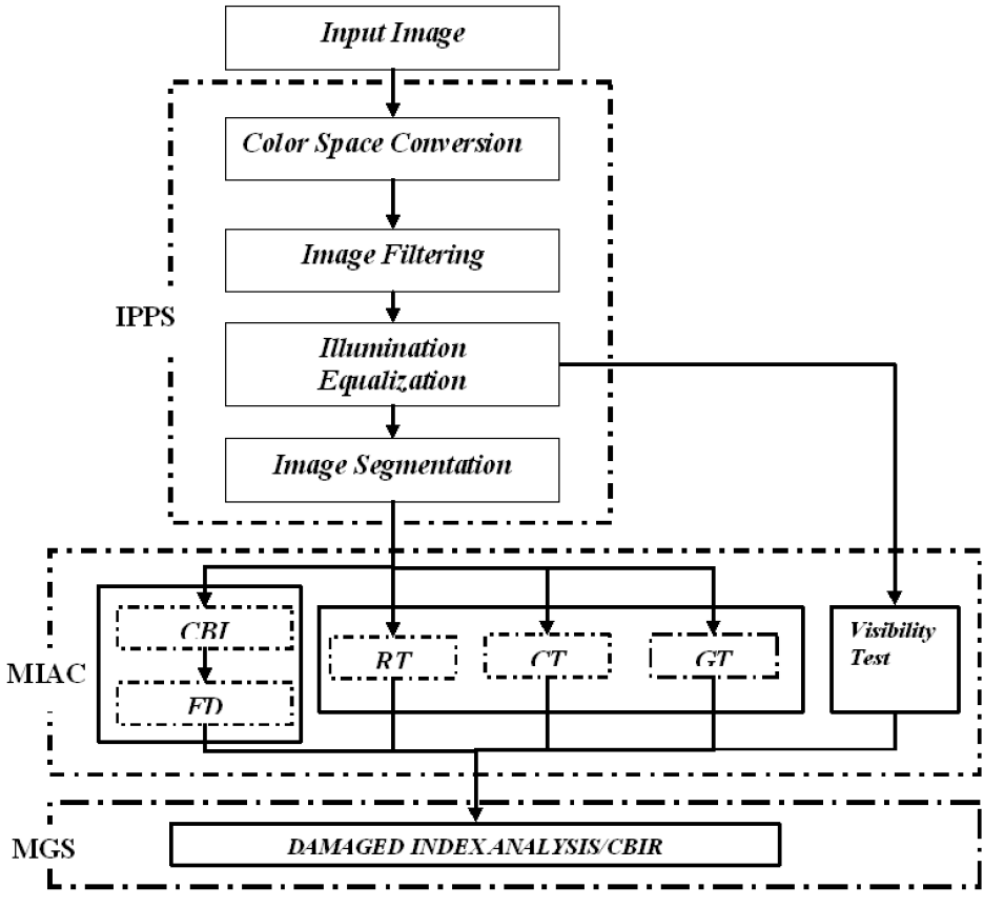

Fig. 4. The block diagram of the proposed technique.

3) Image Filtering:
This involve the application of filter function ($h(n_x; n_y)$) on the grey level MII (x(N,M)). This remove noise in the acquired image and the output image is given by

$$y(n_x, n_y) = \sum_{k_x=1}^{M} \sum_{k_y=1}^{N} x[k_x, k_y] h[n_x - k_x, n_y - k_y] \quad (10)$$

Where N and M are the number rows and columns respectively.

4) Image Intensity Enhancement: Perform intensity matrix enhancement by the use of Global Local Adaptive with Partially Overlapped window (GLAPOW) [13], [24] on the filtered MII. This enhanced image (matrix) also forms part of the input to the the MIAC (Sub section - 3.3 stage.

$$I(N_x, M_y) = F(y(n_x, n_y)) \quad (11)$$

5) Image Segmentation:
It is a partitioning of image I(Nx; My) into two non intersecting, connected, groups of pixels (regions). [23], [24]. It plays an important role in the subsequent stages.

3.2 Spatial Domain Analysis (SDA) stage

The SDA involves the application of a set of geometric related criteria on the segmented MII. These are

- **Ratio Test (RT):** The ratio of the minor axis ($\min(L_S(nx; ny))$ to the major axis $\min(L_S(nx; ny))$ is determined for an infested area by

$$RT = \frac{min(L_S(n_x, n_y))}{max(L_S(n_x, n_y))} \qquad (12)$$

- **Compactness Test (CT):** If a candidate mould region is enclosed in a rectangle, the ratio of the filled area to the total area is also used as a criterion. This is mathematically expressed as

$$CT = \frac{X_S(n_x, n_y)}{X_S(N_x, M_y))} \qquad (13)$$

- **Visibility Test (VT):** This involves the use of intensity matrix obtained as the output of GLAPOW to classify the level of visibility.

$$VT = \begin{cases} 0 & for\ max(I(N_x, M_y)) \leq \theta_1 \\ 0.5 & for\ \theta_1 \leq max(I(N_x, M_y)) \leq \theta_2 \\ 1, & \theta_2 \leq max(I(N_x, M_y)) \end{cases} \qquad (14)$$

Where $ø_1$ and $ø_2$ are thresholds for classifying the images into Less Visible (LVB) (see Fig.??(a)), Visible (VB) (see Fig. 1(a-c)) for visible mould growth).

- **Geometric Test (GT):** This classifies the image and type of mould infestation to Linear (LMI), Radial (RMI) and Disperse (DMI) Mould Images.

- **Eccentricity (EC)**
  Eccentricity is defined as the ratio of the distance between the foci of the ellipse and its major axis length. The value is between 0 and 1. (0 and 1 are degenerate cases; an ellipse whose eccentricity is 0 is actually a circle, while an ellipse whose eccentricity is 1 is a line segment [59]

- **Damage Index Chart**
  Using only CT and RT as reported in [13], the basic DIA test can be obtained and this is as shown in Fig. 5.

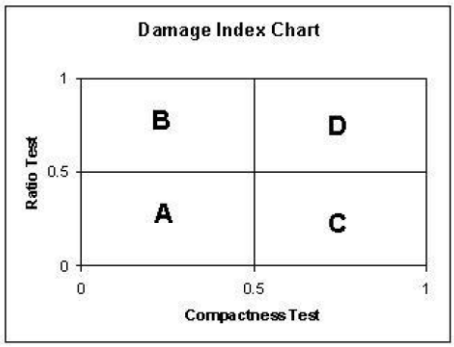

Fig. 5. Damage Index Chart (DIC) for RMI

The interpretations of this Fig. 6 [13] are:
– **DIC Value of A:** CT and RT range from 0:00 to 0:499 means Less Severe mould infestation
[13].
– **DIC Value of B:** CT falls between 0:50 -1:00 and RT falls within 0:00- 0:499 means Moderately Severe mould infested image [13].
– **DIC Value of C**: CT falls between 0:00-0:499 and RT falls within 0:50 - 1:00 means severe mould infested image [13].
– **DIC Value of D**: CT and RT range from 0:50to 1:00 mean Extremely Severe mould infested image [13].

- **Radial Mould Infestation (RMI) Damaged Index**
  Equation The overall Damage Index grading for RMI relating CT, RT and VT is given as

$$DIA_{RMI} = \frac{CT.RT + VT}{2} \qquad (15)$$

where

$$DIA_{RMI} = \begin{cases} 0 & Minimum\ Value \\ 1, & Maximum\ Value \end{cases} \qquad (16)$$

The minimum value corresponds to an image without any mould infestation while the maximum value corresponds to image with highly severe mould growth.

3.3 Frequency Domain Analysis (FDA) stage

FDA involves the application of signatures algorithm (boundary tracing) on the segmented MII, followed by the application of DFT (Eqn. 7) on the resulting signatures. The resulting complex valued FD represent the CBI pixel of the MII but now in frequency domain. These FD coefficients can be stored for future evaluation or comparison in order to monitor mould or fungi growth on such material. The FD can also be used to reconstruct the original binary boundary image by the application of IDFT on the stored FD coefficients. Another merit of this technique is the use of minimal space for storing the coefficients compared to the requirement for storing the acquired MII and for the development of CBIR system. The reconstructed images can be evaluated by measuring the similarities between the original pixel boundary and the reconstructed boundaries using IDFT. The objective image quality criteria used in this work include The Mean square error, randomized mean square error, structural similarity and correlation coefficient.

a) Mean Square Error (MSE)

This involve computing the square of the difference between pixels in two different images and then taken the average over all pixels in the image. An image that

is a perfect reproduction of the original image will have an MSE of zero, while an image that differs greatly from the original image will have a large MSE [60]. The equation for MSE is

$$MSE = \frac{1}{MN}\sum_{y=1}^{N}\sum_{x=1}^{M}|P_{(x,y)} - Q_{(x,y)}|^2 \quad (17)$$

Where M, N are the dimension of the image, P(x;y) is a pixel of the original image and Q(x,y) is the corresponding pixel from the reconstructed image.

b) Randomized Mean Square Error (RMSE)

The RMSE is the square root of Mean Square Error (MSE) [6]. RMSE which is sometimes refers to as Root Mean Square error [4] quantifies the average sum of distortion in each pixel of the reconstructed image. It portrays the average change in a pixel caused by the image-processing algorithm [4].

$$RMSE = \sqrt{MSE}$$

c) Structural Similarity Index (SSI)

The mathematically defined universal quality index [61] models any distortion as a combination of three different factors, namely a) Loss of correlation, b) Luminance distortion; c) Contrast distortion. The dynamic range of SSI is

$$SSI = [-1, +1]$$

The best value 1 is achieved if and only if the two images are similar and -1 if the two images are highly un-similar.

d) Correlation Co-efficient (CC)

Correlation coefficient quantifies the closeness between two images. This coefficient value ranges from -1 to +1, where the value +1 indicates that the two images are highly correlated and are very close to each other. And the value -1 indicates that the images are exactly opposite to each other [60], [62]. The correlation coefficient is given by

$$\frac{\sum_{y=1}^{N}\sum_{x=1}^{M}(P_{(x,y)} - \bar{P}_{(x,y)})(Q_{(x,y)} - \bar{Q}_{(x,y)})}{\sqrt{\sum_{x=1}^{M}\sum_{y=1}^{N}(P_{(x,y)} - \bar{P}_{(x,y)})^2 \sum_{x=1}^{M}\sum_{y=1}^{N}(Q_{(x,y)} - \bar{Q}_{(x,y)})^2}} \quad (18)$$

(a)

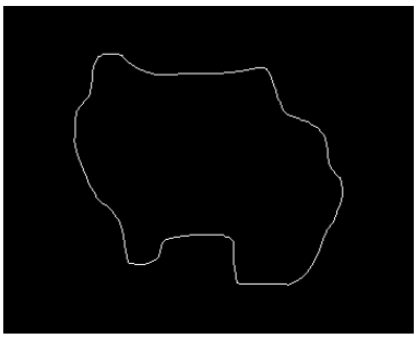

(b)

Fig. 6. Simulated MII-1, (a) IPPS output (b) Boundary image

4. Result obtained

Result obtained by the application of the proposed technique on two types of images, namely simulated and experimental MII is discussed subsequently. Result obtained using four simulated MII (Fig. 6) is as contained in subsection 4.1 while result obtained by application of the proposed technique on experimental MII is as contained in 4.2 respectively.

4.1 Simulated MII

Table III shows the result obtained for the application of the proposed algorithm on a simulated MII shown in Fig. 7 with the boundary plots. Similarly, Fig. 8 shows the centroidal signature plot for Simulated II- 1, the plots shows the relationship between image centroid distance given in (4) and the centered angle.

TABLE I
SDA: Result of DIA for Simulated MII

Im No.	CT	RT	VT	EC	DIA
Simulated MII-1	0.8778	0.6679	0.5000	0.7442	0.5432
Simulated MII-2	0.9756	0.7713	0.5000	0.6365	0.6262
Simulated MII-3	0.8571	0.3920	0.5000	0.9200	0.4180
Simulated MII-4	0.7428	0.0888	0.5000	0.9960	0.2830

a) Simulate MII: SDA Result: Result obtained in
Table III shows the values of CT, RT, EC and VT obtained on the four simulated images. The value of the DIA in the last column of the table can now be used to classify the acquired MII. The eccentricity measure can also be used to segment the acquired image into linear or radial but can't be used to measure the disperse MII.

TABLE II
FDA: Simulated MII similarity measure

# FD	Image No	MSE	RMSE	SSI	CC
10	Simulated MII-1	0.0129	0.1137	0.9995	0.0427
	Simulated MII-2	0.0105	0.1023	0.9997	0.1747
	Simulated MII-3	0.0114	0.1067	0.9997	0.1915
	Simulated MII-4	0.0182	0.1348	0.9994	0.0756
20	Simulated MII-1	0.0118	0.1086	0.9996	0.1418
	Simulated MII-2	0.0068	0.0822	0.9999	0.4707
	Simulated MII-3	0.0076	0.0870	0.9998	0.4786
	Simulated MII-4	0.0146	0.1209	0.9996	0.2661
30	Simulated MII-1	0.0102	0.1008	0.9998	0.2700
	Simulated MII-2	0.0037	0.0605	0.9999	0.7139
	Simulated MII-3	0.0058	0.0761	0.9999	0.6014
	Simulated MII-4	0.0127	0.1125	0.9997	0.3731
40	Simulated MII-1	0.0095	0.0975	0.9998	0.3174
	Simulated MII-2	0.0025	0.0496	1.0000	0.8085
	Simulated MII-3	0.0030	0.0546	0.9999	0.7964
	Simulated MII-4	0.0105	0.1023	0.9996	0.4841
100	Simulated MII-1	0.0090	0.0950	0.9996	0.3568
	Simulated MII-2	0.0001	0.0129	1.0000	0.9871
	Simulated MII-3	0.0005	0.0238	1.0000	0.9613
	Simulated MII-4	0.0027	0.0519	0.9999	0.8680
300	Simulated MII-1	≈ 0.00	0.0044	1.0000	0.9986
	Simulated MII-2	0.0000	0.0000	1.0000	1.0000
	Simulated MII-3	0.0000	0.0000	1.0000	1.0000
	Simulated MII-4	≈ 0.00	0.0099	1.0000	0.9952

b) Simulated MII: FDA Result and Analysis:

- **Choice of signature**

The centered based CVS given in (3) was used as the appropriate signature in this work because it has been shown in the literature to perform better than some of the existing signatures [38], [45]. Furthermore, the centered based CVS is translational invariance and easy to compute hence reason for its adoption in this work. Though centroidal distance can also be used but different mould MII can have the same centroidal plot else it is not as reliable and as accurate as the use of centered based CVS. Furthermore during reconstruction, the effect of Gibb's phenomenon is highly noticeable in the reconstructed centroidal plot (8).

- **Choice of properties**

Rotational invariant FD was obtained by dividing each of the FD coefficients by the DC term, |A (0)| where A(0) is the first non-zero frequency components [50], [56], [57].

$$|\frac{A(1)}{A(0)}|, |\frac{A(2)}{A(0)}|, |\frac{A(3)}{A(0)}| \ldots |\frac{A(N/2)}{A(0)}|$$

Translational invariant is achieved by the use of centered CVS or centroidal distance signature in this work. The value obtained for the |A (0)| shows a close similitude to the analysis obtained during the SDA measure of CT. Hence size invariant was discarded and not given so much prominence in this work.

- **Subjective reconstructed images evaluation**

Visual evaluation of the reconstructed plots shows lots of similarity between the original boundary pixels image and the reconstructed boundary plots. Fig. 9 (a), (b), (c) and (d) shows the reconstructed images using 10, 20, 30 and 40 FD. The result obtained using 30 descriptor (4%) out of the possible 724 descriptors shows shape almost equal to the original shape. Increasing the FD to 40 as shown in Fig 9d does not improve the shape obtained so there is no need for increase in FD beyond 30. The use of 20 descriptors which is almost 3% of the total descriptor shows the image with the principal features of the original image.

- **Measure of similarity**

Table II shows the value obtained from comparing the reconstructed images with the original boundary images. Increasing the number of FD improves the measure of similarity between the original image and the reconstructed image for all the similarity measurement. The MSE, RMSE and SSIM show relative same poor performance when compared to the use of CC. It can also be observed from the FD analysis that once the mould shape has little corners or contour (e.g. Simulate MII-2) very few numbers of FD is enough to reconstruct or describe the shape whereas same number of FD might not be sufficient to describe same shape with high number of contour. The mathematical explanation for this is that FD used in this work are basically low frequency FD and such low frequency coefficients are only responsible for the global mould shape information while high frequency components are responsible for the contour and fine detail in the boundary image.

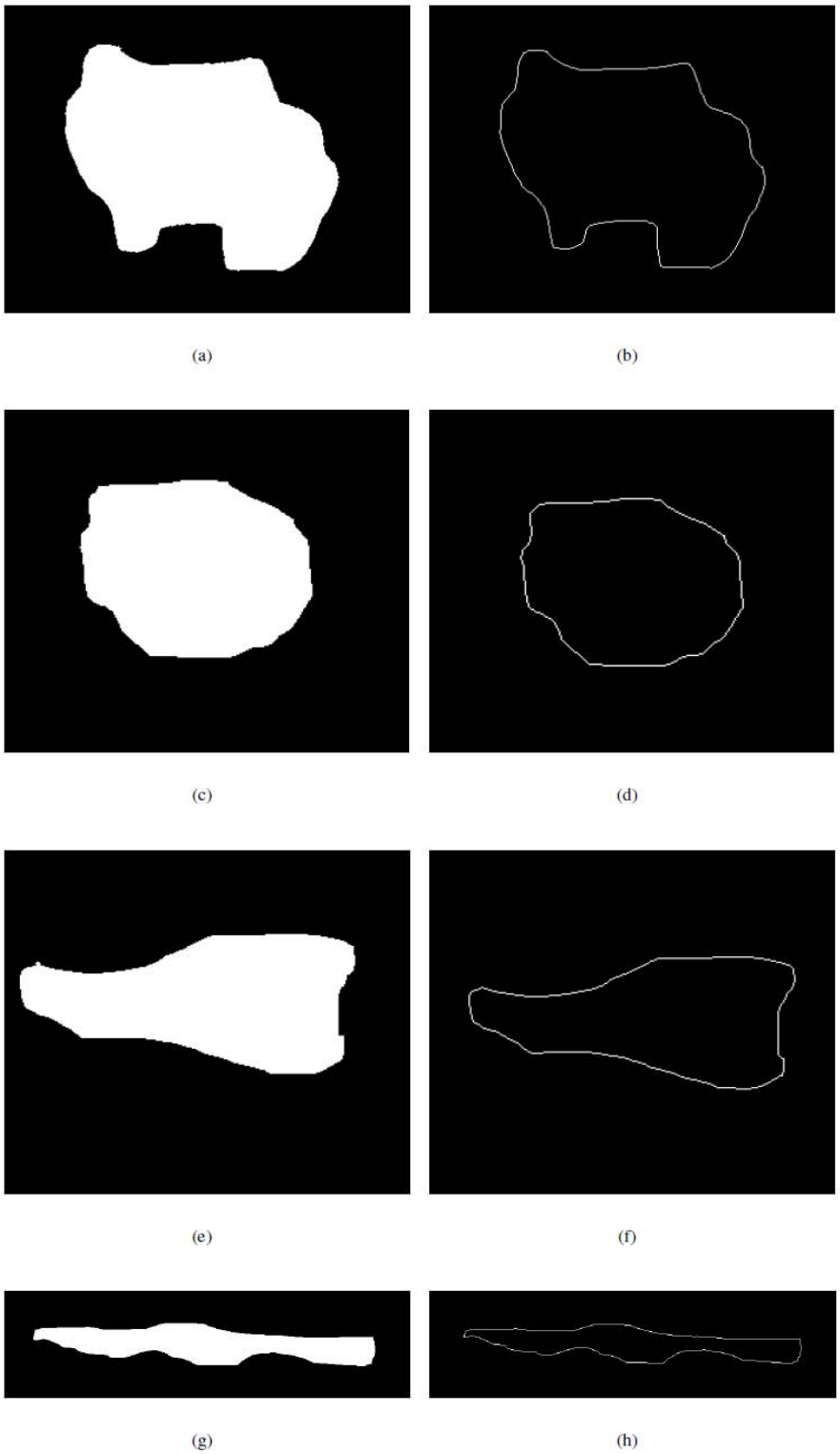

Fig. 6. a) Simulated MII -1, (b)Boundary plot for Simulated MII -1, (c) Simulated MII -2, (d)Boundary plot for Simulated MII-2, (e) Simulated MII -3 (f)Boundary plot for Simulated MII -3, (g) Simulated MII -4 (h)Boundary plot for Simulated MII -4

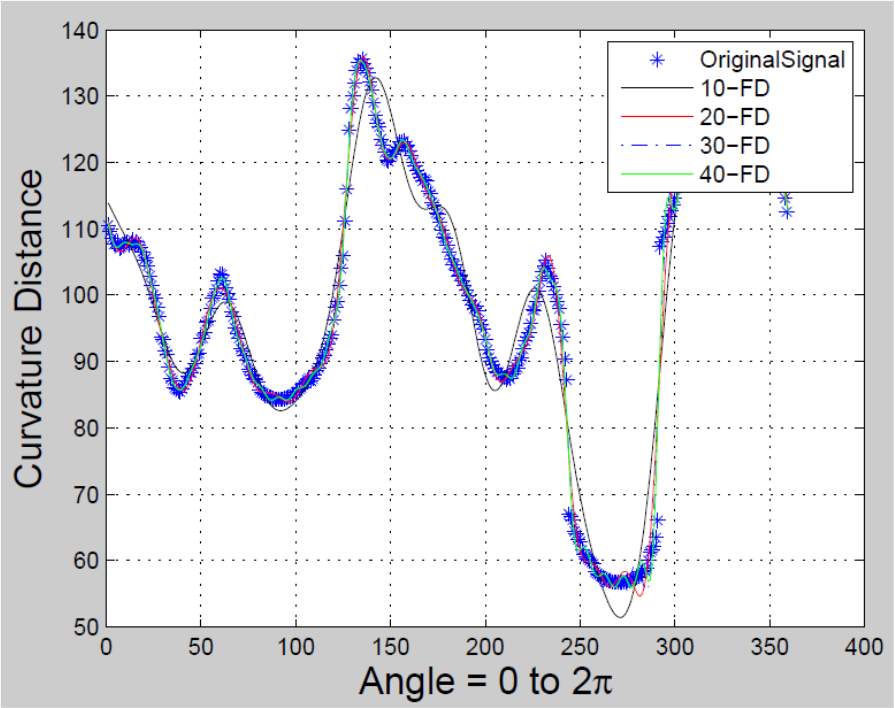

Fig. 8. Centroidal plot of the Simulated MII

4.2 Experimental Images

Result obtained by the application of proposed technique on experimental MII is as shown in Table III. The objective output obtained provides a means of quantifying and analyzing mould infested materials by the use of DIA and the use of Eqn. 15. Similar results were obtained for experimental MII hence detail discussion can be avoided. The output of MGS for the four different images is as tabulated

Below:

TABLE III
SDA: DIA result for experimental MII

Im No.	CT	RT	VT	DIA
Image-1	0.370	0.351	0.500	0.315
Image-2	0.344	0.628	0.500	0.358
Image-3	0.379	0.540	1.000	0.602
Image 4	0.000	0.0000	0.000	0.000

Table III indicates the level of mould infestation on a grading of 0-1 for Image-1 and Image-2 as 0.315 and 0.358 respectively. Result for Image-3 shows high degree of infestation while result obtained for Image-4 shows that the material is yet to be infested with mould.

5. Conclusion

In this paper, a new method of objective evaluation of the degree of mould infestation on building materials using spatial and frequency domain analysis has been proposed. The input data was obtained from digital camera and subsequent application of digital image processing, digital signal processing technique and shape analysis on the acquired MII provides a grading value needed in assessing the level of mould infestation on such materials. Also proposed in this paper is an equation relating the overall damaged index value to the spatial domain analysis of mould infested area.

Another area of contribution of this research work is the proposed mould classification scheme using image intensity and spatial domain boundary information of the acquired image. The application of the popular frequency domain based Fourier theory on the acquired MII shows that the use of FD provide more information that its counterparts in the spatial domain. More so, the use of less than 10% of the resulting FD can be used to reconstruct the original spatial domain boundary image with high structural similarity and correlation. The limitation in this work is that the proposed methodology is only applicable to CBI that is either LMI or RMI in nature.

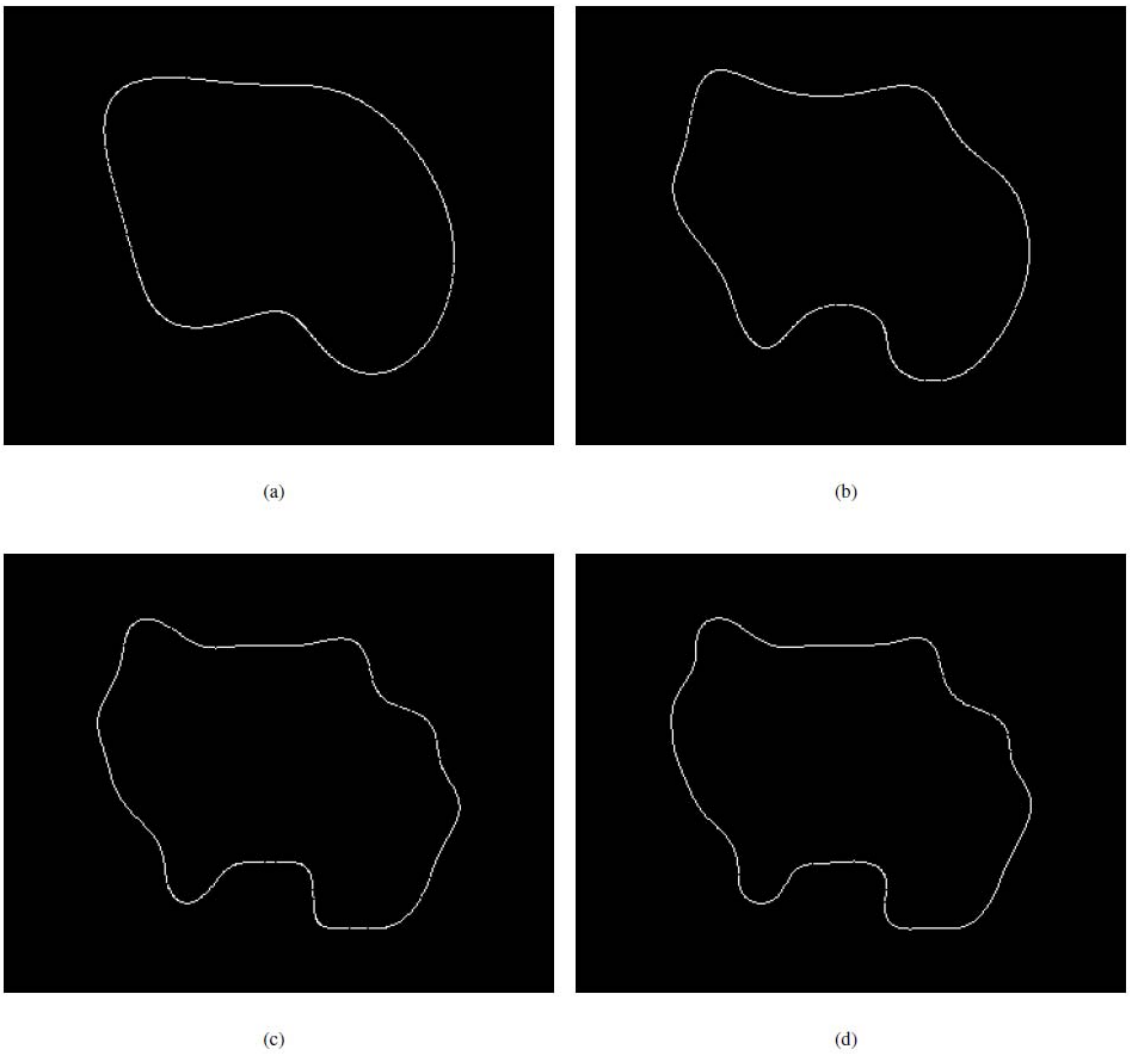

Fig. 9. Reconstructed SMII Using (a) 10 FD, (b) 20 FD,(c) 30 FD (d) 40 FD out of possible 724 FD

References

[1] I. A Bamgbopa " Assessment of Moulds Growth in Hospitals Indoor Enviroement: HVAC System Aspect" Unpublished Msc Thesis, International Islamic University Malaysia, 2008.

[2] L. A. Rode, "Mold identification and prevention In Wisconsin schools".Unpublished Master dissertation .University of Wisconsin Stout 2002.

[3] G. J Johansen, "Litigating Mould claims crisis ? What crisis ".Journal of Land Use, Vol.19:2, pp 465-4892004.

[4] T. Godish, "Indoor environmental Quality". Lewis Publishers, USA, 2000.

[5] www.aiha.org/GovernmentAffairs-PR/html/oomold.htm

[6] J. A. Scott, "Studies on Indoor Fungi". Unpublished PHD dissertation Department of Botany in the University of Toronto, Canada, 2001.

[7] E.A Arens and A. Baughman " Indoor humidity and human health: part II -buildings and their system." http:/repositories.cdlib.org , Acessed 8th January, 2008.

[8] H. Chen, S. Deng, H. Bruner, and J. Garcia, "Root of mold problems and humidity control measures in institutional buildings with preexisting mold condition", Proceedings of the twelfth symposium on improving building systems in hot and humid climates, San Antonio, Texas. Https://Txspace.Tamu.Edu/Bitstream/Handle/1969.1/4605/Esl-Hh-04-05-07.Pdf?Sequence=1 Retrieved 31st Dec. 2007

[9] K.F Nielsen, "Mycotoxin production by indoor molds," Fungal Genetics and Biology 39: 103-117, 2003.

[10] E. Torvinen, T. Meklin, P. Torkko, S. Suomalainen, R. Marjut,M.L Katila, L. Panlin and A. Nevalainen, "Micro bacteria in moisture damaged building materials". Applied and environmental microbiology , Vol 72, no 10, 2006.

[11] L. Harriman and B. Nelson, "Mold and Humidity Control Design Guide For Commercial And Institutional Buildings", ASHRAE Pp 100- 121, 2001.

[12] P. Haisley, "Field inspection protocol for investigation of mold damaged buildings", Unpublished PhD Dissertation, School of Architecture, University of Hawaii,2002.

[13] I. A. Bamgbopa, A. M Aibinu, M.J.E Salami, A. A. Shafie, M. Ali and P.S. Jahn Kassim, " Damage Index analysis: Mould growth analysis using Digital image Processing technique ", Proceeding of International Conference on Computer and Communication Engineering, Malaysia, pp -584:588 May, 2008.

[14] L. Curtis, A. Lieberman, M. Stark, W. Rea, and M. Vetter, "Adverse Health Effects of Indoor Molds" Journal of Nutritional & Environmental Medicine, Vol. 14(3), 261-274, 2004.

[15] G. Richardson, S. Eick, S and R. Jones, "Integrative Literature Reviews And Meta-Analyses How Is The Indoor Environment Related To Asthma?: Literature Review" Journal Of Advanced Nursing, 52(3), 328-339. 2005 Blackwell Publishing Ltd.

[16] E. Pieckova E and Z. Jesenska, "Microscopic fungi in dwellings and their health implications in humans", Ann. Agric environ med. 6,1-11, 1999.

[17] S. Gravesen, P. A. Nielsen, R. Iverson, and K. F Nielsen, " Micro fungal contamination of damp building materials-example of risk constructions and risk materials", Environmental health perspective, vol.107, supplement 3.505-508,1999.

[18] W. S. K Frank, " Perceived Air quality : Investigation of the nonsensory odor assessment in indoor environment". Unpublished PhD Thesis, Technical University of Berlin, 2000.

[19] E. Karunasena, N. Markham, T. Brasel, J.D Cooley and D.C Straus, "Evaluation of fungal growth on cellulose -containing and inorganic ceiling tile. " Mycopathology, 150: 91-95, 2000.

[20] K.F Nielsen, "Moulds growth on building materials .secondary metabolites, Mycotoxin and biomarkers," Unpublished PHD thesis. Technical university of Denmark.

[21] E. Pieckova and Z. Jesenska, "Microscopic fungi in dwellings and their health implications in humans," Ann. Environ. Med 6: 1-11, 1999.

[22] U. Haverinen, M. Vahferisto, J. Pekkanen, T. Husman, A. Nevalainen and D. Moschhandreas, "Formulation and validation of an Empirical Moisture Damage Index," environmental modeling and assessment . Kluwer academic publishers,8: 303-309 2003.

[23] R. C. Gonzalez, R. E. Woods and S. L. Eddins, "Digital Image Processing Using MATLAB", 2nd edition, ISBN 0-201-18075-8, Prentice Hall, 2002.

[24] A. M. Aibinu, M. I. Iqbal, M. Nilsson and M. J. E. Salami, "A New Method of Correcting Uneven Illumination Problem in Fundus Images", International Conference on Robotics, Vision, Information, And Signal Processing, Penang, Malaysia, pp. 445 - 449, Nov. 2007.

[25] Nielsen, K.F., Holm, G., Uttrup, L.P., and Nielsen, P.A. "Moulds growth on building materials under low water activities. Influence of humidity and temperature on fungal growth and secondary metabolism. International biodeteroriation and biodegradation". Vol 54, pg. 325-336,2004.

[26] Burge, H.A., Su, J.H., and Spengler, J.D. . Moisture, organisms, and health effects. In Treschsel H.R, (Ed.). Manual on moisture control in buildings. American society for testing and material (ASTM) USA. Pg84-90,1994.

[27] Adan, O. C .G. On the fungal defacement of interior finishes PhD Thesis, Eindhoven University of Technology,1994.

[28] Torvinen, E., Meklin. T., Torkko, P., Suomalainen, S., Reiman, .M., Katila, M., Paulin, L.,and Nevalainen, A. (2006). Mycobacteria And Fungi In Moisture-Damaged Building Materials. Applied and environmental microbiology, vol. 72, No 10. pp. 6822-6824.

[29] Haisley, P. (2002). Field inspection protocol for investigation of mold damaged buildings. Unpublished PhD Dissertation. School of Architecture. University of Hawaii

[30] Karunasena, E., Markham, N., Brasel, T., Cooley, J.D., and Straus, D.C. (2000). Evaluation of fungal growth on cellulose-containing and inorganic ceiling tile. Mycopathologia 150: 91-95.

[31] Gorny, R.L.; Dutkiewicz, J. and Traczyk, E.K. (1999). Size distribution of bacterial and fungal Bioaerosols in indoor air. Ann. Agric Environ. Med.vol 6: 105-113.

[32] Sautour et al., ; Sautour, M., Sixt, N., Dalle, F., L'olliver, .C., Calinon, C., Fouquenent,. V., Thibaut, C., Jury, H., Lafon, .L, Aho, S., Couillaut, G., Vagner, O., Cuisenier, B., Besancenot, J.P., Caillot, D., and Bonnin, A. (2007). Prospective survey of indoor fungal contamination in hospital during a period of building construction. Journal of Hospital Infection vol 6, 367-373, 2007.

[33] Havener, G (2004). Effective Investigation and Control of an Aspergillosis Outbreak in a Regional Burn Unit. Retrieved December 31, 2007.
[34] Anaissie, E. J., Stratton, S. L, Dignani, M. C., Lee, C., Summerbell, R. C., Rex, J. H., Monson, T. P.and Walsh, T. J. . Pathogenic Molds (Including aspergillus Species) In Hospital Water Distribution Systems: A 3-Year Prospective Study and Clinical Implications for Patients with Hematological Malignancies. Retrieved December 31, 2007.
[35] Arvanitodou, M., Kanellou, K., Constantinides, T.C., and Katsouyannopoulos, V. The Occurrence of Fungi in Hospital and Community Potable Waters. The Society For Applied Microbiology, Letters In Applied Microbiology 29, 81-84, 2004
[36] Johansen, G.J. (2004). Litigating Mold Claims Crisis? What Crisis? Journal of Land Use, Vol. 19:2, Pg 465-489. Retrieved
[37] A new tool for assessment of mould growth on building materials: Aibinu et al., (2009)
[38] H. Kauppinen, T. Seppanen, and M. Pietikainen, "An Experimental comparison of autoregressive and fourier-based descriptors in 2D shape classification", IEEE PAMI , vol. 17, no. 2, pp. 201207, 1995.
[39] S Xiong and Z Zhou, " A complex Nonlinear Exponential Autoregressive Model Approach to Shape Recognition Using Neural Network ", in IEEE Trans. on Instruments and Measurements, Vol. 49, No. 6 pp. 1298-1304, Dec. 2000.
[40] I. Sekita, T. Kurita and N. Otsu," Complex Autoregressive Model for Shape Recognition", in IEEE Trans. on Pattern Analaysis and Machine Intelligence, Vol. 14, No. 4 pp. 489-496, 1992.
[41] B. Kartikeyan and A. Sarkar, "Shape Description by Time Series", in IEEE Trans. on Pattern Analaysis and Machine Intelligence, Vol. 11, No. 9 pp. 489-496, Sep. 1989.
[42] C. Liu and N. Ahuja, " A model for Dynamic Shape and Its Applications", IEEE Trans. , 2004.
[43] R. L. Kashyap and R. Chellappa, "Stochastic Models for Closed Boundary Analysis , Representation and Reconstruction", in IEEE Trans. on Information Theory, Vol. IT-27, No. 5 pp. 627-637, Sep. 1981.
[44] D. Zhang and G. Lu, " A Comparative Study of Fourier Descriptors for Shape Representation and Retrieval", in The 5th Asian Conf. on Computer Vision, pp. 1-6 , Jan. 2002.
[45] D. Zhang and G. Lu, " Review of Shape Representation and Description Techniques", in Elsevier, The Journal of the Pattern Recognition Society, Vol. 37, pp.1-19 , 2004.
[46] S. R. Dubois and F. H. Glanz, "An Autoregressive Model Approach to Two Dimensional Shape Classification", in IEEE Trans. on Pattern Analaysis and Machine Intelligence, Vol. PAM1-8, No. 1 pp. 55-66, Jan. 1986.
[47] R. Gonzalez and R. Woods, "Digital Image Processing", Prentice-Hall Inc., 2002.
[48] L. Costa and R. M Cesar Jr., "Shape Analysis and Classification", CRC Press, 2001.
[49] I. A. Bamgbopa, A. M Aibinu, M.J.E Salami, A. A. Shafie, M. Ali and P.S. Jahn Kassim, " Damage Index analysis: Mould growth analysis using Digital image Processing technique ", Proceeding of International Conference on Computer and Communication Engineering, Malaysia, pp - 584:588 May, 2008.
[50] A. F. Abtae, M. Nappi, D. Riccio and S. Ricciardi, " Ear Recognition by means of a Rotational Invariant Descriptor", Proc. of 18th Int. Conf. on Pattern Recognition , 2006.
[51] A. El-Ghazal, O. Basir and S. Belkasim, " A new Shape Signature For Fourier Descriptor", ICIP-2007, 2007.
[52] M. Zhenjiang, M.H Gandelin and Y. Baozong, " Fourier Based Image Shape Analysis and Its Application to Flower Recognition", ICSP- 2002, 2007.
[53] M. H. Mahoor and M. Abdel-Mottaleb, " Automatic Classification of Teeth in BITEWING Dental Image", ICIP-2004, pp. 3475-3478, 2004.
[54] H. Jia and M. Xie, " Improvement of Fourier Descriptor Using Spatial Normalization", IEEE ISCIT-2005, pp. 1237-1240, 2005.
[55] H. Wu, P. Zhou and Z. Gao, " An Algorithm for Automatic Side Face Portrait Recognition based on Fourier Descriptor", IEEE Int. Symp. on Info. Sci and Engr, 2008, pp. 767-772, 2008.
[56] N. Tahir, A. Hussain, and M. Mustafa, " Fourier Descriptor for Pedestrian Shape Recognition usig Support Vector Machine ", IEEE Int. Symp. on Signal Proc. and Info. Tech., 2007, pp. 636-640, 2007.
[57] I. Kunttu and L. Lepstio, "Shape-based retrieval of Industrial Surface defects using angular radius Fourier Descriptor ", IET, 2007, pp. 231- 236, 2007.
[58] Z. Wang, Z. Chi, and D. Feng, " Shape based leaf Image Retrieval ", *IEE proc. Vis. Image Signal Process., Vol 150, No. 1 2003, pp. 34-43, 2003.*
[59]: MATLAB toolboox.
[60] G. P. Mulopulos, A. A. Hernandez and L. S. Gasztonyi "Peak Signal to Noise Ratio Performance Comparison of JPEG and JPEG 2000 for Various Medical Image Modalities", *Symposium on Computer June, 2003.*
[61] B. Shrestha, C.G. O'Hara and N. H. Younan, JPEG2000: IMAGE QUALITY METRICS", ASPRS 2005 *Annual Conference, Baltimore, Maryland March 7-11, 2005.*
[62] Z. Wang, Z. Chi, and D. Feng, " Shape based leaf Image Retrieval ", *IEE proc. Vis. Image Signal Process., Vol 150, No. 1 2003*, pp. 34-43, 2003.